Inorganic Chemistry

Article

pubs.acs.org/IC

Field-Induced Ferromagnetism and Multiferroic Behavior in End-on Pseudohalide-Bridged Dinuclear Copper(II) Complexes with Tridentate Schiff Base Blocking Ligands

Subrata Jana,[†,⊥] Bikash Kumar Shaw,[‡,⊥] Prasanta Bhowmik,[†] Klaus Harms,[§] Michael G. B. Drew,[∥] Shouvik Chattopadhyay,*[,†] and Shyamal Kumar Saha*[,‡]

[†]Department of Chemistry, Inorganic Section, Jadavpur University, Kolkata - 700 032, India

[‡]Department of Materials Science, Indian Association for the Cultivation of Science, Kolkata - 700 032, India

[§]FachbereichChemie, Philipps-Universität Marburg, Hans-Meerwein-Straße, 35032 Marburg, Germany

[∥]School of Chemistry, The University of Reading, P.O. Box 224, Whiteknights, Reading RG6 6AD, United Kingdom

Supporting Information

ABSTRACT: Four new end-on pseudohalide-bridged dinuclear copper(II) complexes, $[Cu_2(L^1)_2(N_3)_2]\cdot DMF$ (**1**), $[Cu_2(L^2)_2(N_3)_2]$ (**2**), $[Cu_2(L^3)_2(NCS)_2]$ (**3**), and $[Cu_2(L^4)_2(N_3)_2]$ (**4**) {where HL^1, HL^2, HL^3, and HL^4 are tridentate N_2O donor Schiff bases}, are synthesized and characterized. Complexes **1**, **2**, and **3** possess $\pi\cdots\pi$ stacking interactions, while in addition hydrogen-bonding interactions are present in **1** and **3**. However, by contrast, complex **4** contains neither type of interaction. Field-induced long-range ferromagnetic ordering beyond 0.9 T is observed in complexes **1** and **2** due to $\pi\cdots\pi$ stacking interactions, while ferroelectric ordering is observed in complexes **1** and **3** due to hydrogen-bonding interactions. Most interestingly, complex **1**, which contains both $\pi\cdots\pi$ stacking and hydrogen-bonding interactions, shows multiferroic behavior as a result of coupling between the dielectric and magnetic fields with 8% change in the magneto−dielectric effect at room temperature. We believe that from this study will emerge a new class of multiferroic materials.

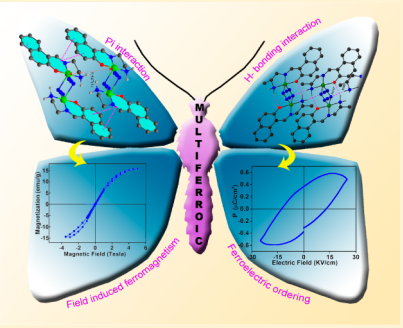

1. INTRODUCTION

The study of magnetic interaction in coordination complexes is an interesting area of research because of their fundamental importance as well as technological applications. The magnetic interactions in such complexes mainly occur due to super exchange coupling between the metal centers via bridging ligands, and the strength and nature of this interaction whether ferromagnetic or antiferromagnetic depends on the bridging moiety and its subtended angle. Intensive research has already been carried out on several polynuclear complexes having versatile bridging ligands, and the correlation between geometry and magnetic properties has been investigated.[1]

Although magnetic interactions between metal centers through superexchange coupling have been studied exhaustively in a large number of polynuclear metal centers with different bridging ligands and subtended angles, long-range ferromagnetic ordering in these systems is very rare. The main hindrance to achieving this long-range ordering is the weak coupling that exists between molecules in spite of possessing strong intramolecular coupling. Therefore, to achieve long-range ferromagnetic ordering it is essential to have strong intramolecular coupling as well as strong intermolecular ordering. Several strategies have been developed to increase intermolecular coupling, such as the creation of hydrogen-bonding and $\pi\cdots\pi$ stacking interactions. It is seen that metal centers connected through bridging ligands via hydrogen bonds are coupled through either ferromagnetic or antiferromagnetic interactions based on the nature of hydrogen bonds.[2] However, the magnetic interaction between metal centers ($S = 1/2$) connected through aromatic moieties via strong $\pi\cdots\pi$ stacking interactions depends upon the stacking angle and interaction between the spin densities of the stacked layers.[3]

From the different bridging ligands, azides have attracted particular attention in recent years in the field of molecular magnetism because of possible variations in geometry. The azido ligand has several coordination modes, with the *end-on* ($\mu_{1,1}$) and *end-to-end* ($\mu_{1,3}$) being the most common. It is also well established that the magnetic coupling strongly depends on the coordination mode of the azide ligand. Thus, the $\mu_{1,1}$ bridging mode gives rise to ferromagnetic coupling when the M−N−M angle is 104° or less, while the $\mu_{1,3}$-N_3 bridge generates strong antiferromagnetic coupling.[4] These variations have been exploited to prepare azido-bridged complexes of transition metals showing diverse magnetic interactions viz. ferromagnetic and antiferromagnetic couplings, metamagnetism,[5] spin canting,[6] spin flop,[7] and even single-molecule magnets[8] and single chain magnets.[9]

Received: June 10, 2014
Published: August 1, 2014

   dx.doi.org/10.1021/ic501353g | *Inorg. Chem.* 2014, 53, 8723−8734

Therefore, keeping all these aspects in mind, in the present work, we have synthesized four new end-on pseudohalide-bridged dinuclear Cu(II) complexes $[Cu_2(L^1)_2(N_3)_2]\cdot DMF$ (**1**), $[Cu_2(L^2)_2(N_3)_2]$ (**2**), $[Cu_2(L^3)_2(NCS)_2]$ (**3**) and $[Cu_2(L^4)_2(N_3)_2]$ (**4**) using four different N_2O donor tridentate Schiff bases, HL^1, HL^2, HL^3 and HL^4, as blocking ligands. The Schiff bases, HL^1 and HL^3, are so designed that they are capable of forming H-bonding, and as a result, their complexes (**1** and **3**) form supramolecular chain via interdimer H-bonding. On the other hand, $\pi\cdots\pi$ stacking interactions are present in **1**, **2**, and **3**. However, neither H-bonding nor $\pi\cdots\pi$ stacking interactions are present in complex **4**. The unique advantage of forming a complex containing both strong $\pi\cdots\pi$ stacking interactions which gives rise to ferromagnetism[10] and hydrogen-bonding interactions which provide a ferroelectric response[11] is the possibility of invoking multiferroic behavior which arises due to coupling between the magnetic dipole and the electric dipole.

In previous work, we have reported temperature-induced long-range ferromagnetic ordering at room temperature due to $\pi\cdots\pi$ stacking interactions between bipyridine ligands.[12] As a result of this observation, it is interesting to note that tuning of $\pi\cdots\pi$ stacking in coordination complexes due to thermal energy or magnetic field energy has provided a new topic in the field of molecular magnetism. Therefore, in the present work we have explored the observation of field-induced ferromagnetic ordering in complexes **1** and **2** due to long-range interdimer $\pi\cdots\pi$ stacking interactions, whereas 1-D long-range H-bonding interaction results in the ferroelectric ordering in complexes **1** and **3**. The combination of long-range $\pi\cdots\pi$ stacking interactions as well as H-bonding interactions in complex **1** leads to the generation of multiferroic behavior. Indeed a significant magneto−dielectric effect beyond the applied magnetic field of 0.8 T where field-induced ferromagnetic ordering is initiated is observed in complex **1**.

2. EXPERIMENTAL SECTION

All chemicals were of AR grade and were used as purchased from Sigma-Aldrich without further purification.

2.1. Preparations. **Caution!** Although our samples never exploded during handling, metal complexes with azide are potentially explosive; only a small amount of material should be prepared and handled with great care.

Synthesis of $[Cu_2(L^1)_2(N_3)_2]\cdot DMF$ (1). A solution of 2-hydroxy-1-naphthaldehyde (0.172 g, 1 mmol) in methanol (20 mL) was added to a methanol solution (25 mL) of copper(II) acetate monohydrate (0.2 g, 1 mmol), and immediately the solution turned green. A methanol/water solution (5 mL) of sodium azide (0.065 g, 1 mmol) was then added, and the resulting mixture was stirred for 30 m. A methanol solution (5 mL) of 1,2-diaminopropane (0.085 mL, 1 mmol) was added slowly to the mixture and stirring was continued for 10 m. The mixture was then refluxed for 45 m and filtered to remove a small amount of precipitate that appeared immediately. The filtrate was kept in open atmosphere, and X-ray diffraction quality, dark-green, block-shaped, single crystals were obtained from DMF solution after few days on slow evaporation in open atmosphere.

Yield: 0.45 g (61%), Anal. Calc for $C_{31}H_{37}Cu_2N_{11}O_3$ (FW 738.79): C, 50.40; H, 5.05; N, 20.85; Found: C, 50.4; H, 5.1; N, 20.9%. IR (KBr, cm^{-1}) 1621 ($\nu_{C=N}$), 2042 (ν_{N3}), 3236, 3284 (υ_{N-H}); UV−vis, λ_{max} (nm) [ε_{max} (dm^3 mol^{-1} cm^{-1})] (Methanol) 317 (32716), 382 (20624), 605 (407).

Synthesis of $[Cu_2(L^2)_2(N_3)_2]$ (2). A methanol solution (20 mL) of *N*,*N*-dimethyl-1,3-diaminopropane (0.13 mL, 1 mmol) and 1-hydroxy-2-acetonaphthone (0.186 g, 1 mmol) was refluxed for ∼1 h to prepare the tridentate Schiff base, HL^2. The ligand was not isolated and used directly for the synthesis of complex **2**. A methanol solution (20 mL) of copper(II) acetate monohydrate (0.2 g, 1 mmol) was added to the methanol solution of the ligand and stirred for 1 h. A methanol/water solution (5 mL) of sodium azide (0.065 g, 1 mmol) was then added and stirred further for ∼1 h. A black precipitate separated out and was collected by filtration. Diffraction quality single crystals were obtained after a few days on slow evaporation of a dark-green acetonitrile solution of the complex in open atmosphere.

Yield: 0.43 g (64%), Anal. Calc for $C_{34}H_{42}Cu_2N_{10}O_2$ (FW 749.88): C, 54.46; H, 5.65; N, 18.68; Found: C, 54.5; H, 5.7; N, 18.7%. IR (KBr, cm^{-1}) 1584 ($\nu_{C=N}$), 2040 (ν_{N3}); UV−vis, λ_{max} (nm) [ε_{max} (dm^3 mol^{-1} cm^{-1})] (Methanol) 322 (17503), 385 (18511), 530 (802).

Synthesis of $[Cu_2(L^3)_2(NCS)_2]$ (3). Complex **3** was prepared in a way similar to that of complex **1**, except that 1,2-diaminoethane (0.074 mL, 1 mmol) and sodium thiocyanate (0.081 g, 1 mmol) were used instead of 1,2-diaminopropane and sodium azide, respectively. X-ray diffraction quality single crystals were obtained from the mother liquor after few days on slow evaporation in open atmosphere.

Yield: 0.43 g (64%), Anal. Calc for $C_{28}H_{26}Cu_2N_6O_2S_2$ (FW 669.75): C, 50.21; H, 3.91; N, 12.55; Found: C, 50.2; H, 3.9; N, 12.6%. IR (KBr, cm^{-1}) 1623 ($\nu_{C=N}$), 2069 (ν_{SCN}), 3275, 3224 (υ_{N-H}); UV−vis, λ_{max} (nm) [ε_{max} (dm^3 mol^{-1} cm^{-1})] (Methanol) 315 (27217), 384 (18491), 608 (417).

Synthesis of $[Cu_2(L^4)_2(N_3)_2]$ (4). A methanol solution (20 mL) of *N*,*N*-diethyl-1,2-diaminoethane (0.14 mL, 1 mmol) and 2-hydroxy-1-acetonaphthone (0.186 g, 1 mmol) was refluxed for ∼1 h to prepare the tridentate Schiff base, HL^4. The ligand was not isolated and used directly for the synthesis of complex **4**. A methanol solution (20 mL) of copper(II) acetate monohydrate (0.2 g, 1 mmol) was added to the methanol solution of the ligand (1 mmol) and stirred for 1 h. A methanol/water solution (5 mL) of sodium azide (0.065 g, 1 mmol) was then added and stirred further for ∼1 h. A black precipitate separated out and was collected by filtration. Diffraction quality single crystals were obtained after a few days by slow evaporation of a dark-green acetonitrile solution of the complex in open atmosphere.

Yield: 0.43 g (64%), Anal. Calc for $C_{36}H_{46}Cu_2N_{10}O_2$ (FW 777.93): C, 55.58; H, 5.96; N, 18.01; Found: C, 55.6; H, 5.9; N, 18.1%. IR (KBr, cm^{-1}) 1611 ($\nu_{C=N}$), 2064 (ν_{N3}); UV−vis, λ_{max} (nm) [ε_{max} (dm^3 mol^{-1} cm^{-1})] (Methanol) 296 (34549), 373 (14543), 598 (762).

2.2. Physical Measurements. Elemental analysis (carbon, hydrogen, and nitrogen) was performed using a Perkin-Elmer 240C elemental analyzer. IR spectra in KBr (4000−500 cm^{-1}) were recorded using a Perkin-Elmer spectrum two FT-IR spectrophotometer. Electronic spectra in methanol (800−200 nm) were recorded in a Jasco V-630 spectrophotometer at 298 K. Fluorescence spectra in methanol were recorded on a Shimadzu RF-5301PC spectrofluorophotometer at room temperature.

SQUID magnetometer (Quantum Design MPMS) was used to investigate the magnetic properties (magnetic susceptibility (field cooled magnetization/FCM) and M−H measurements). Temperature-dependent permittivity over 298−515 K and magneto−dielectric measurements (using an electromagnet supplied by M/S control systems and devices; Mumbai, India) were performed with the Agilent E4980A Precision LCR meter. The polarization study was carried out using Radiant's Precision Premier II ferroelectric tester. Dielectric permittivity and polarizibility were measured by the standard two-probe technique using powdered sample pressed in the form of a pellet with 0.5 cm^2 area and 0.06 cm in thickness. Good contact was made by highly conducting silver adhesive and fine copper wires as electrodes.

X-ray Crystallography. Single crystals of complexes **1** and **3** were used for data collection using a 'Bruker D8 QUEST area detector' and "STOE IPDS" diffractometer equipped with graphite-monochromated Mo Kα radiation (λ = 0.71073 Å) at 100 K, respectively.

Single crystals of complexes **2** and **4** were used for data collection using an 'Oxford Diffraction X-Calibur System' diffractometer equipped with graphite-monochromated Mo Kα radiation (λ = 0.71073 Å) at 150 K.

For all four complexes, molecular structures were solved by direct methods and refinement by full-matrix least-squares on F^2 using the SHELXL-97 package.[13] Non-hydrogen atoms were refined with anisotropic thermal parameters. Hydrogen atoms were placed in

dx.doi.org/10.1021/ic501353g | Inorg. Chem. 2014, 53, 8723−8734

Table 1. Crystal Data and Refinement Details of Complexes

complex	1	2	3	4
formula	$C_{31}H_{37}Cu_2N_{11}O_3$	$C_{34}H_{42}Cu_2N_{10}O_2$	$C_{28}H_{26}Cu_2N_6O_2S_2$	$C_{36}H_{46}Cu_2N_{10}O_2$
formula weight	738.79	749.88	669.75	777.93
crystal size [mm]	0.22 × 0.07 × 0.04	0.17 × 0.17 × 0.23	0.08 × 0.09 × 0.15	0.16 × 0.18 × 0.22
temperature (K)	100	150	100	150
crystal system	monoclinic	monoclinic	triclinic	triclinic
space group	$P2_1/c$	$P2_1/c$	$P\bar{1}$	$P\bar{1}$
a (Å)	5.9467(6)	10.4117(4)	7.7560(12)	8.8163(9)
b (Å)	19.2537(16)	14.8906(6)	8.1836(11)	9.4155(9)
c (Å)	28.013(2)	11.9038(5)	10.7113(13)	12.5851(10)
α (deg)	(90)	(90)	93.394(11)	70.450(8)
β (deg)	92.605(5)	113.976(5)	97.360(11)	89.450(8)
γ (deg)	(90)	(90)	90.01(12)	68.980(9)
Z	4	2	1	1
d_{calc} (g cm^{-3})	1.532	1.477	1.653	1.417
μ (mm^{-1})	1.380	1.309	1.775	1.214
$F(000)$	1528	780	342	406
total reflections	30534	11486	5234	6500
unique reflections	5908	4906	2488	5110
observed data [$I > 2\sigma(I)$]	4377	4163	1454	4228
no. of parameters paraparameters	444	220	188	229
R(int)	0.088	0.034	0.059	0.024
R1, wR2 (all data)	0.0851, 0.1092	0.0478, 0.0971	0.0725, 0.0724	0.0588, 0.1120
R1, wR2 [$I > 2\sigma(I)$]	0.0541, 0.0998	0.0381, 0.0914	0.0354, 0.0664	0.0453, 0.1007
max, min residual electron density e/Å^3	0.629, −0.393	0.418, −0.758	0.501, −0.418	0.449, −0.499

their geometrically idealized positions and constrained to ride on their parent atoms. Empirical absorption corrections were applied to **2** and **4** using the ABSPACK program.[14] Other programs used included SIR92,[15] PLATON,[16] and X-AREA.[17] Crystallographic data are given in Table 1.

3. RESULTS AND DISCUSSION

3.1. Synthesis. The formation of the complexes **1** and **3** can be rationalized in light of the templating effect of copper(II) modulated by the counteranions. The templating agents contain the necessary information to arrange an assembly of building blocks so that they can be linked together in a specific manner.[18] The azide or thiocyanate has crystal field stabilization energy approximately similar to that of the Schiff bases and occupies one coordination site of copper(II), leaving the other three sites to be coordinated by a Schiff base, and that can be achieved by "half-salen" type tridentate Schiff base ligand. In the present work, the "half-salen" type monocondensed Schiff base ligands, HL^1 and HL^3, were synthesized conveniently as the copper(II) complexes, $[Cu_2(L^1)_2(N_3)_2]\cdot DMF$ (**1**) and $[Cu_2(L^3)_2(NCS)_2]$ (**3**) by the reaction of 2-hydroxy-1-naphthaldehyde, copper(II) and sodium azide (for **1**) or sodium thiocyanate (for **3**) followed by the reaction with 1,2-diaminopropane (for **1**) or 1,2-diaminoethane (for **3**). In the absence of azide or thiocyanate, tetradentate Schiff base ligands are formed, produced by the 1:2 condensations of the respective diamines with 2-hydroxy-1-naphthaldehyde, which form four-coordinate square planar complexes (Scheme 1). The structures of these complexes have been reported in the literature.[19]

On the other hand, HL^2 and HL^4 were prepared straightforwardly following the literature method.[20] Addition of copper(II) acetate and sodium azide in the methanol solution of the ligands produced complexes **2** and **4**, respectively (Scheme 2).

Scheme 1. Synthesis of Complexes 1, 3, and Some Related Complexes

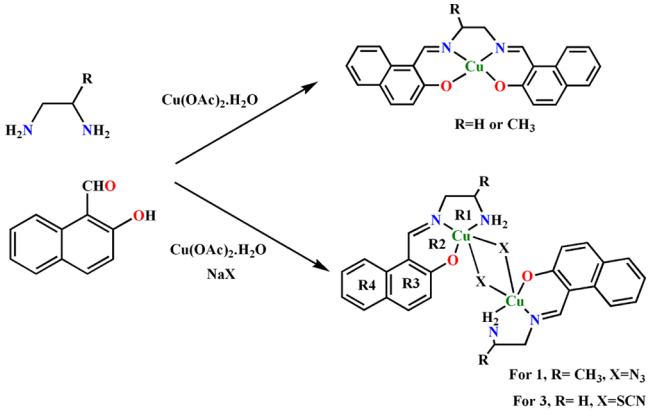

R1, R2, R3, R4 indicate the corresponding chelate and phenyl rings in complexes 1 and 3

Scheme 2. Synthesis of Complexes 2 and 4

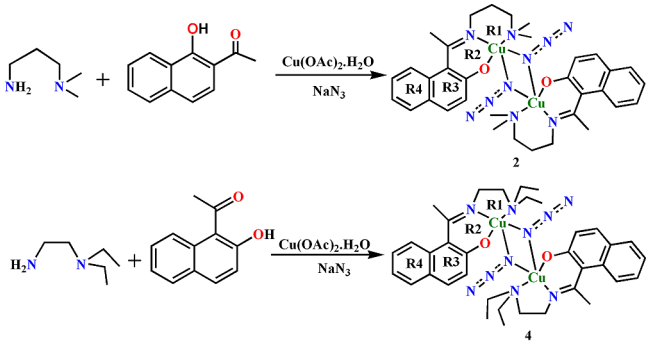

R1, R2, R3, R4 indicate the corresponding chelate and phenyl rings in complexes 2 and 4

dx.doi.org/10.1021/ic501353g | Inorg. Chem. 2014, 53, 8723−8734

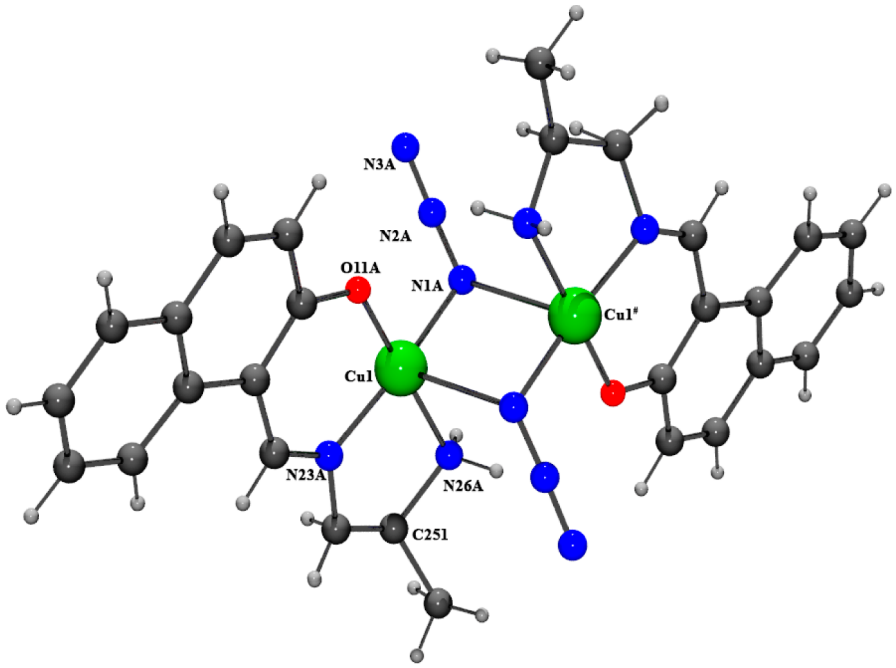

Figure 1. Perspective view of the centrosymmetric complex **1A** with selective atom numbering scheme. The structure of **1B** is equivalent. The chiral carbon, C(251), has been labeled.

3.2. Descriptions of the Structures. All four structures are centrosymmetric dimers in which the two copper(II) are five-coordinate being bonded to three donor atoms (O, N, N) of the specific Schiff base ligand and two $\mu_{1,1}$ bridging anionic ligands, azide in **1**, **2**, and **4** and thiocyanate in **3**. The geometry of the copper coordination spheres varies considerably in the four complexes between square pyramidal and trigonal bipyramidal although all are closer to the former geometry. Assuming that geometry, the three donor atoms of the Schiff base occupy the equatorial plane, while each of the two anionic ligands in the dimer occupy an equatorial position in one metal coordination sphere and an axial position at a longer distance in the other.

The bond lengths in the equatorial plane are very similar in the four complexes. Cu−O distances range from 1.898(3)−1.918(2) Å, while the Cu−N(imine) distances are significantly shorter at 1.911(3)−1.947(2) Å than the Cu−N(amine) distances at 2.003(3)−2.124(2) Å. The Cu−N(anion) bond length in the equatorial plane is 1.964(4)−2.009(2) Å. The Cu−N(anion) axial bond lengths range from 2.374(2)−2.734(4) Å.

*$[Cu_2(L^1)_2(N_3)_2]\cdot DMF$ (**1**).* The structure of complex **1** contains two independent units (called **A** and **B**) both with crystallographic centers of symmetry. A perspective view of molecules **A** and **B** are shown together with the atom numbering scheme respectively in Figures 1 and S1 in the Supporting Information (SI). In both molecules the saturated ring is disordered and the two carbon atoms in the ring are disordered over two sites with occupation ratios of 0.67(1), 0.33(1) in **A** and 0.63(1), 0.37(1) in **B**.

The Addison parameter[21] (trigonality index, $\tau = (\alpha - \beta)/60$, where α and β are the two largest L−M−L angles of the coordination sphere) is 0.061, 0.088 in **A** and **B**, respectively, and this confirms the square−pyramidal character ($\tau = 0$ for a perfect square pyramid and a $\tau = 1$ for a perfect trigonal bipyramid). As usual for a square pyramid structure, the copper center is slightly pulled out of the least-squares plane toward the apical donor atom at a distance 0.033(1) Å in molecule **A** and 0.048(1) Å in molecule **B**. Deviations of the coordinating atoms, N(23), N(26), N(1), and O(11) from the least-squares basal plane are −0.148(4), 0.142(4), −0.135(4), and 0.141(3) Å, respectively, in **A** and −0.105(2), 0.101(2), −0.100(2), 0.101(2) Å, respectively, in **B**. The bond lengths to the azide are 1.985(4), 1.995(3) Å in the equatorial plane and 2.646(4), 2.577(3) Å in the axial position in **A** and **B**, respectively.

The five-membered chelate ring, R1 {Cu(1)−N(23)−C(24)−C(25)−N(26)} assumes a twist-boat conformation with puckering parameters $Q(2) = 0.460(7)$ Å and $\phi(2) = 264.8(5)°$ in **A** and 0.398(9) Å and 91.8(7)° in **B**.[22] The bond lengths and angles are comparable with those for the related copper(II) complexes.[23] The bridging $Cu_2(N)_2$ network is perforce planar. The bridging azide anions are quasi-linear with the N−N−N angle being 178.5(1)° and 177.9(1)° in **A** and **B**, respectively. The intradimer Cu···Cu distance is 3.179(1) Å in **A** and 3.182(1) Å in **B**. The selected bond lengths and angles are shown in Table S1 in the SI.

The hydrogen atoms, H(26A) and H(26B), attached to N(26A) are involved in hydrogen-bonding interactions with the symmetry-related phenoxo oxygen atom, O(11A)[a] ([a] = 2−x, −y, 1−z) and azide nitrogen atom, N(1A)[b] ([b] = 2−x, 1−y, 1−z), respectively, to form a one-dimensional chain along the crystallographic a axis, as shown in Figure 2.

Similarly, H(26C) and H(26D) attached to N(26B) form hydrogen bonds with O(11B) and N(1B). Dimensions of these four hydrogen bonds are given in Table 2.

One methylene hydrogen atom, H(24E), attached to C(243) is involved in an intermolecular C−H···π interaction with the symmetry-related (−1+x,y,z) phenyl ring R4B and one aromatic hydrogen atom, H(17B), attached to C(17B) is involved in C−H···π interaction with the symmetry related (x, 1/2−y, 1/2+z) phenyl ring R4A to form a two-dimensional sheet, as shown in Figure S5 (SI). On the other hand, the unsaturated six-membered chelate ring, R2, is involved in intermolecular $\pi\cdots\pi$ interaction with the symmetry-related

dx.doi.org/10.1021/ic501353g | Inorg. Chem. 2014, 53, 8723−8734

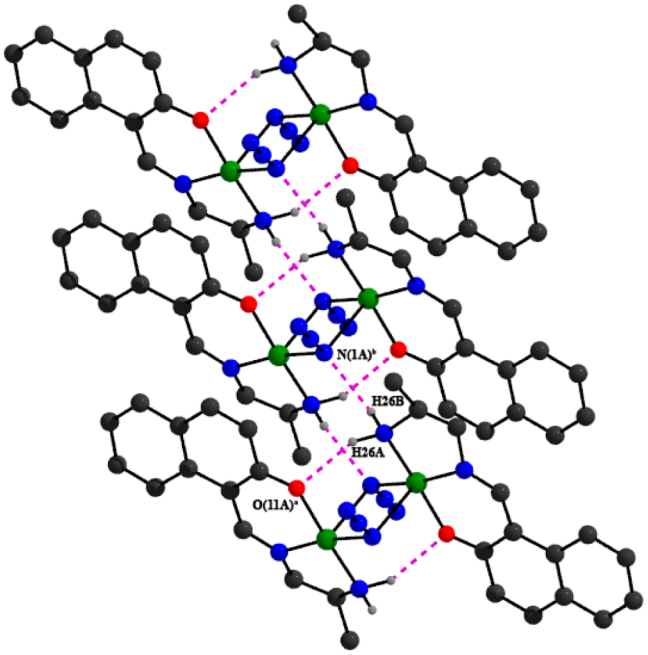

Figure 2. One-dimensional H-bonded structure of complex **1**. Only relevant hydrogen atoms are shown. Hydrogen bonds are shown as dotted lines.

(−1+*x*, *y*, *z*) phenyl rings, R3 and R4, forming a one-dimensional chain (Figure 3). Geometric features of the C−H···π and π···π interactions are given in Tables S2 and S3 in the SI. There is a DMF solvent molecule in the asymmetric unit, but it does not form any significant supramolecular interactions.

*$[Cu_2(L^2)_2(N_3)_2]$ (**2**).* A perspective view of the centrosymmetric dimeric complex **2** with the selective atom numbering scheme is shown in Figure S2 in the SI. The selected bond lengths and angles are shown in Table S1 in the SI. Here the saturated ring contains an extra methylene group compared to **1** (and indeed **3** and **4**) which leads to significant differences in geometry from the other structures.

The Addison parameter is 0.46, indicating a geometry almost exactly intermediate between square pyramidal and trigonal bipyramidal. Assuming a square pyramid, the copper(II) is slightly directed from the mean squares plane toward the apical donor atom at a distance of 0.2391(2) Å. Deviations of the coordinating atoms N(1), O(11), N(23), and N(27) from the least-squares equatorial plane are −0.324(2), 0.351(2), −0.325(2), and 0.298(2) Å, respectively. The axial and equatorial Cu−N bond lengths are 2.374(2), 2.009(2) Å respectively. The six-membered chelate ring, R1{Cu(1)−N(23)−C(24)−C(25)−C(26)−N(27)}, assumes a twist-boat conformation with puckering parameters Q(2) = 0.830(2) and

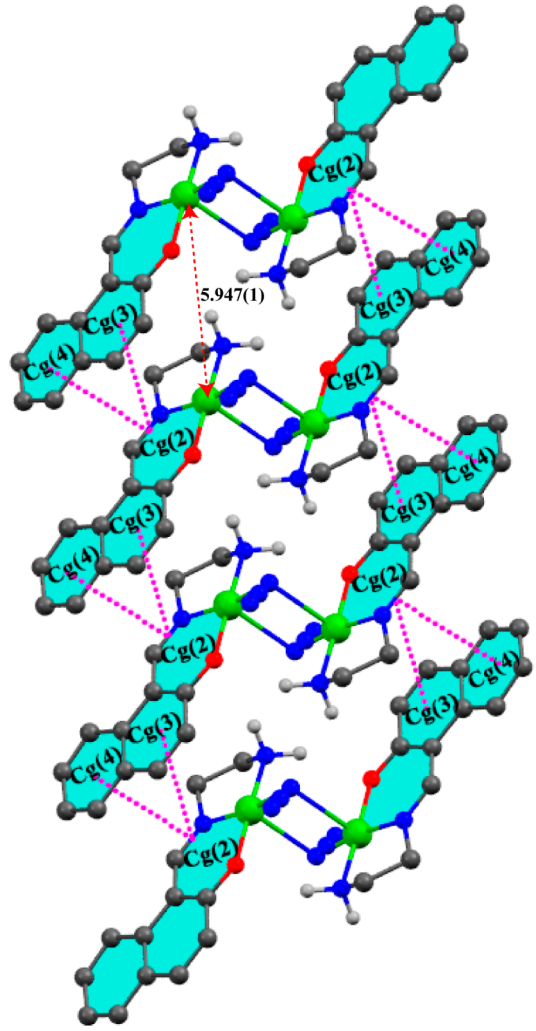

Figure 3. One-dimensional chain of complex **1A** via π···π interactions. Hydrogens bonded to carbon are omitted for clarity. The structure of **1B** is equivalent.

$\phi(2)$ = 257.77(12).[22] The bond lengths and angles are comparable with those for the related copper(II) complexes.[23] The intradimer Cu···Cu distance is 3.426(1) Å, considerably longer than that found in complex **1**, no doubt because of the more distorted coordination sphere.

There are no significant hydrogen-bonding interactions in the complex. One methyl hydrogen atom, H(22C), attached with C(221) is involved in an intermolecular C−H···π interaction with the symmetry related (1−*x*, −*y*, −*z*) phenyl ring R4. Similarly, one methylene hydrogen atom, H(25B), attached with C(25) is involved in C−H···π interactions with

Table 2. Hydrogen Bond Distances (Å) and Angles (deg) in Complexes 1 and 3[a]

complexes	D−H···A	D−H	D···A	H···A	∠D−H···A
1	N(26A)−H(26A)···O(11A)[b]	0.92	3.087(5)	2.24	152
	N(26A)−H(26B)···N(1A)[c]	0.92	3.186(5)	2.50	131
	N(26B)−H(26F)···O(11B)[d]	0.92	3.158(5)	2.33	149
	N(26B)−H(26E)···N(1B)[e]	0.92	3.189(5)	2.51	130
3	N(26)−H(26B)···O(11)[f]	0.80	3.063(4)	2.36	147
	N(26)−H(26A)···S(3)[g]	0.80	3.645(4)	2.88	161

[a](D, donor; H, hydrogen; A, acceptor, symmetry transformation. [b]= 1−*x*,1−*y*,1−*z*. [c]= −*x*, 1−*y*. [d]= −1−*x*,−*y*,1−*z*. [e]= −*x*,−*y*,1−*z*. [f]= 2−*x*,−*y*,1−*z*,1−*z*. [g]= 2−*x*,1−*y*,1−*z*.).

dx.doi.org/10.1021/ic501353g | *Inorg. Chem.* 2014, 53, 8723−8734

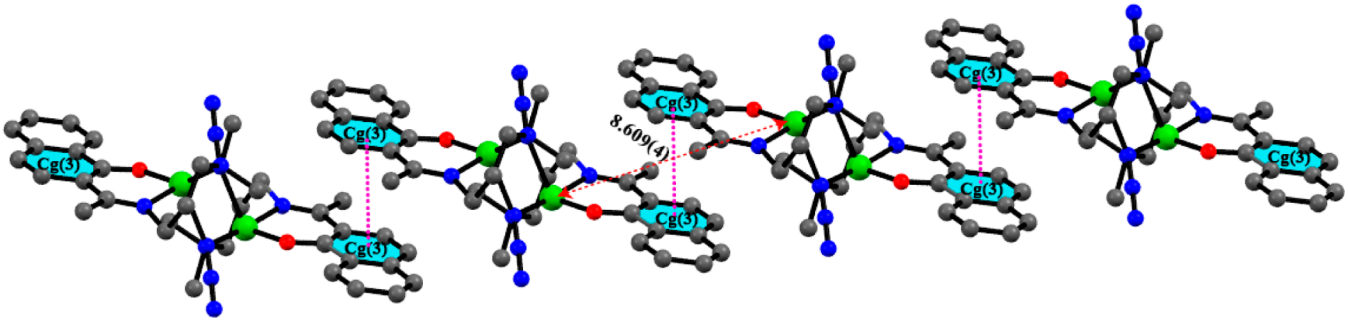

Figure 4. One-dimensional chain of complex **2** via $\pi\cdots\pi$ interactions. Hydrogen atoms are omitted for clarity.

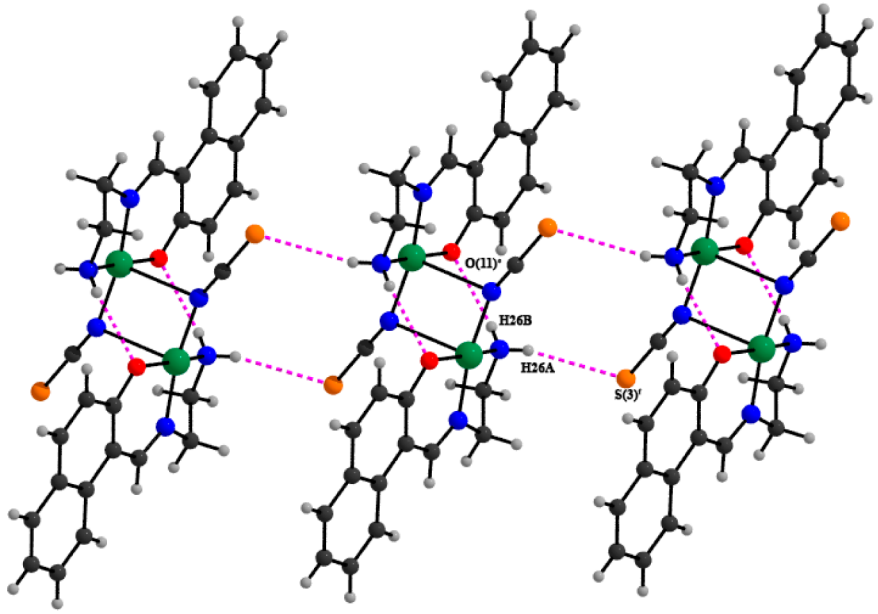

Figure 5. One-dimensional H-bonded structure of complex **3**. Hydrogen bonds are shown as dotted lines.

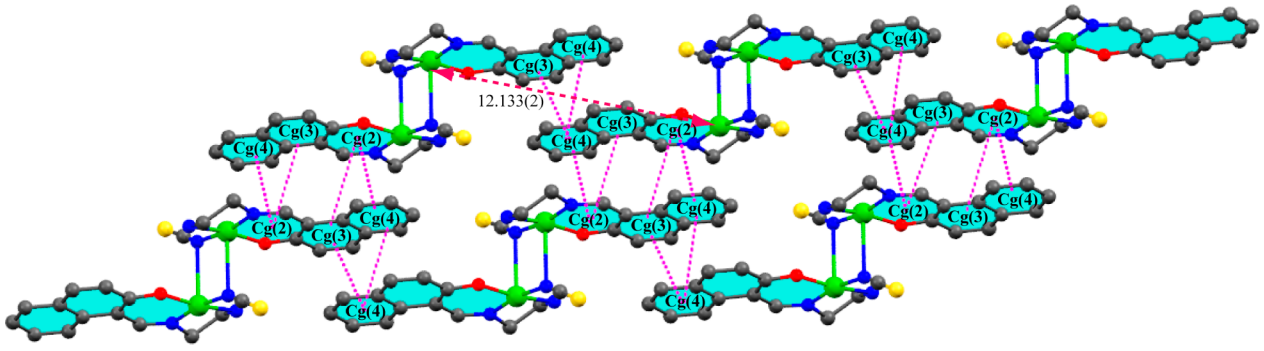

Figure 6. Two-dimensional layer of complex **3** formed via $\pi\cdots\pi$ interactions. Hydrogen atoms omitted for clarity.

the symmetry-related (x,1/2−y,1/2+z) phenyl ring, R3 forming a three-dimensional network (Figure S6, SI). The phenyl ring R3 is involved in an intermolecular $\pi\cdots\pi$ interaction with symmetry-related (1−x,−y,−z) phenyl ring R3 forming a one-dimensional chain along crystallographic a axis (Figure 4). Geometric features of the C−H$\cdots\pi$ and $\pi\cdots\pi$ interactions are given respectively in Tables S2 and S3 in the SI.

*$[Cu_2(L^3)_2(NCS)_2]$ (**3**).* Complex **3**, also a centrosymmetric dimer, is shown in Figure S3 in the SI together with the selective atom numbering scheme. Selected bond lengths and angles are shown in Table S1 in the SI.

The Addison parameter is 0.002, and this confirms the ideal square−pyramidal character of the coordination sphere. Here the copper(II) is found within the equatorial plane with a deviation of 0.003(1) Å. The Cu−N bond lengths in axial and equatorial positions are 2.734(4), 1.964(4) Å. This very long axial bond is no doubt concomitant with the fact that the copper(II) is not distorted from the equatorial plane. Deviations of the coordinating atoms N(23), N(26), N(1), and O(11) from the least-squares basal plane are 0.166(3), −0.160(3), 0.152(3) and −0.158(2) Å, respectively. The five-membered ring, R1 {Cu(1)−N(23)−C(24)−C(25)−N(26)},

dx.doi.org/10.1021/ic501353g | *Inorg. Chem.* 2014, 53, 8723−8734

Table 3. Geometric Features (distances in Å and angles in deg) of the $\pi\cdots\pi$ Interactions Obtained for 1, 2, and 3[a]

complex	Cg (ring I) ··· Cg (ring J)	D_p	α	β	γ	$D1_p$	$D2_p$	symmetry element of ring J
1A	Cg(2)···Cg(3)	4.152(3)	7.06(18)	32.23	38.51	3.2491(15)	3.5124(18)	−1+*x*,*y*,*z*
	Cg(2)···Cg(4)	4.258(3)	10.6(2)	33.48	43.12	3.1082(15)	3.551(2)	−1+*x*,*y*,*z*
1B	Cg(2)···Cg(3)	4.179(2)	5.38(17)	31.56	36.30	3.3683(14)	3.5611(17)	−1+*x*,*y*,*z*
	Cg(2)···Cg(4)	4.120(3)	6.7(2)	31.40	35.94	3.3354(14)	3.516(2)	−1+*x*,*y*,*z*
2	Cg(3)···Cg(3)	3.834(1)	0	23.76	23.76	3.5088(8)	3.5088(8)	1−*x*,−*y*,−*z*
3	Cg(2)···Cg(3)	4.002(2)	0.42(16)	32.55	32.87	3.3613(13)	3.3734(16)	2−*x*,−*y*,−*z*
	Cg(2)···Cg(4)	3.470(2)	1.14(16)	14.75	15.30	3.3465(13)	3.3552(17)	2−*x*,−*y*,−*z*
	Cg(3)···Cg(4)	3.628(2)	0.72(19)	21.68	21.74	3.3701(16)	3.3715(17)	2−*x*,−1−*y*,−*z*
	Cg(4)···Cg(4)	3.762(2)	0	26.67	26.67	3.3619(17)	3.3618(17)	2−*x*,−1−*y*,−*z*

[a] α = Dihedral Angle between rings I and J (deg); β = Angle between Cg(I) → Cg(J); γ = Angle between Cg(I) → Cg(J) vector and normal to plane J (deg); D_p = distance between the centroids of ring I and ring J; $D1_p$ = perpendicular distance of Cg(I) to ring J; $D2_p$ = perpendicular distance of Cg(J) to ring I. Rings are identified in Schemes 1 and 2. For complex **1**, Cg(2), Cg(3), and Cg(4) are the centers of gravity of rings R2, R3, and R4; for complex **2**, Cg(3) is the center of gravity of ring R3. For complex **3**, Cg(2), Cg(3), Cg(4) are the centers of gravity of rings R2, R3, and R4.

Table 4. Parameters Obtained from the Fitting Procedure of Variable-Temperature Magnetic Susceptibility Data

complex	*g*	$2J$ (cm^{-1})	Θ (K)	TIP	R^2
$C_{28}H_{30}Cu_2N_{10}O_2,C_3H_7NO$ (**1**)	2.12	+19.2	+0.44	4.7×10^{-3}	4.9×10^{-5}
$C_{34}H_{36}Cu_2N_{10}O_2$ (**2**)	2.13	−24.7	−5.7	2.66×10^{-3}	2.8×10^{-4}
$C_{28}H_{26}Cu_2N_6O_2S_2$ (**3**)	2.11	+4.1	−0.4	2.95×10^{-6}	4.6×10^{-5}
$C_{36}H_{46}Cu_2N_{10}O_2$ (**4**)	2.12	−11.4	−0.52	0	5.1×10^{-5}

assumes a twist-boat conformation with puckering parameters $Q(2) = 0.427(2)$ and $\phi(2) = 127.2(2)$. The bond lengths and angles are comparable with those for the related copper(II) complexes.[23] The bridging $Cu_2(N)_2$ network is perforce planar. The bridging NCS^- anions are quasi-linear; the N−C−S angle is 178.55(2)°. The intradimer Cu···Cu distance is 3.238(1) Å.

The hydrogen atoms, H(26A) and H(26B), attached to N(26) are involved in hydrogen-bonding interactions with the symmetry-related phenoxo oxygen atom, O(11)[c] ([c] = 2−*x*,−*y*, 1−*z*) and symmetry-related thiocyanate sulfur atom, S(3)[d] ([d] = 2−*x*,1−*y*,1−*z*), respectively, to form a one-dimensional chain along the crystallographic *b* axis, as shown in Figure 5. Details of hydrogen bonding are given in Table 2. The unsaturated chelate ring R2, is involved in intermolecular $\pi\cdots\pi$ interactions with the symmetry-related (2−*x*,−*y*,−*z*) phenyl rings, R3 and R4. Similarly, the phenyl ring R4 is involved in intermolecular $\pi\cdots\pi$ interactions with symmetry related (2−*x*,−1−*y*,−*z*) phenyl rings R3 and R4, forming a two-dimensional sheet, as shown in Figure 6. Geometric features of the $\pi\cdots\pi$ interactions are given in Table 3.

*$[Cu_2(L^4)_2(N_3)_2]$ (**4**).* This complex is also a centrosymmetric dimer as shown in Figure S4 in the SI together with the selective atom numbering scheme. Selected bond lengths and angles are listed in Table S1 in the SI. The Addison parameter is 0.34, showing that the geometry around copper(II) is distorted between square pyramidal and trigonal bipyramidal but closer to the former. Considering the former geometry, the copper(II) is slightly pulled out of the mean squares plane toward the apical donor atom at a distance 0.167(1) Å. Deviations of the coordinating atoms N(1), O(11), N(23), and N(26) from the least-squares basal plane are 0.368(2), −0.428(2), 0.435(2), and −0.375(2) Å, respectively. The five-membered chelate ring, R1 {Cu(1)−N(23)−C(24)−C-(25)−N(26)}, assumes a half-chair conformation with puckering parameters $Q(2) = 0.435(2)$ and $\phi(2) = 121.4(3)$.[22] The bond lengths and angles are comparable with those for the related copper(II) complexes.[23] The intradimer Cu···Cu distance is 3.370(1) Å.

Two methylene hydrogen atoms, H(24A) attached with C(24), and H(27A) attached with C(27), are involved in intramolecular C−H···π interactions with the symmetry-related (1−*x*,−*y*,1−*z*) phenyl rings, R3 and R4, forming a chain-like structure along crystallographic *b* axis, as shown in Figure S7 (SI). Geometric features of the C−H···π interactions are given in Table S2 in the SI.

3.3. IR, Electronic and Fluorescence Spectra. In the IR spectra of all the complexes, distinct bands due to the azomethine (C═N) group are observed around 1600 cm^{-1}. The presence of the azides in complexes **1**, **2**, and **4** is confirmed by intense bands around 2100 cm^{-1}. On the one hand, the appearance of a strong band at 2069 cm^{-1} in the IR spectrum of **3** indicates the presence of thiocyanate. The bands around 3290 cm^{-1} in the IR spectra of the complexes **1** and **3** are due to N−H bond stretching vibrations.

All complexes show absorption bands in the UV region due to ligand-to-metal charge transfer transitions. The broad absorption bands in the visible region (~600 nm) due to d-d transitions are observed for all complexes. All complexes show fluorescence at room temperature in methanol solution upon excitation at ~300 nm. Details of the excitation and emission wavelengths are given in Table S3 in the SI.

3.4. Magnetic Studies. Magnetic measurements have been carried out on all four crystalline complexes **1**−**4**. The temperature-dependent magnetic susceptibility (field-cooled magnetization) of complexes **1**−**4** is investigated under the applied magnetic field of 100 Oe over the temperature range from 2−300 K as shown in Figure S8 in the SI. The inset in Figure S8 in the SI reveals that this susceptibility curve increases upon cooling and rises suddenly at lower temperatures for all complexes. The $\chi_M T$ value at room temperature varies from 0.72 to 1.33 $cm^3\ mol^{-1}$ K, which is in the range close to the value observed in magnetically coupled binuclear copper systems.

The experimental data for magnetic susceptibility with temperature of all four complexes **1**−**4** are fitted in the form of the variation of $\chi_M T$ vs T using the theoretical expression of dinuclear systems given by −

dx.doi.org/10.1021/ic501353g | Inorg. Chem. 2014, 53, 8723−8734

$$\chi_M = \frac{2N\beta^2 g^2}{k(T-\theta)}[3 + \exp(-2J/kT)]^{-1} + N\alpha \quad (1)$$

where N, β, and k are constants and have their usual significance. $N\alpha$ is the temperature-independent paramagnetism. The values of g, θ, and $2J$ (singlet−triplet energy gap) parameters, and the corresponding agreement factors (R^2), $\sum T^2 (\chi_{obs} - \chi_{cal})^2 / \sum T^2 (\chi_{obs})^2$ obtained from the least-squares fitting procedure, are summarized in Table 4.

Figure 7 displays the variation of $\chi_M T$ as a function of temperature for complexes **1** and **2**. For complex **1**, the $\chi_M T$ value increases smoothly down to 4 K and then falls sharply, resulting in a susceptibility maximum of 1.31 cm^3 mol^{-1} K, as shown in Figure 7a. This behavior is indicative of the ferromagnetic exchange coupling operating between the intradimer copper(II) ions, stabilizing the triplet state instead of the singlet state. From the fitted curve, it is clearly seen that the susceptibility follows a weak ferromagnetic exchange pathway with positive exchange coupling constant, $2J$ = 19.2 cm^{-1}. The value of $\chi_M T$ decreases until 300 K as the ground state of superexchange coupling between the copper(II) centers in the dimer remains ferromagnetic up to 300 K. The magnetic behavior in dinuclear copper systems is mainly dominated by super exchange coupling phenomenon of either ferromagnetic or antiferromagnetic type, depending upon their bridging atom as well as the angle and distance between the bridged copper centers. Generally for the azide-bridged dinuclear copper systems, the ferromagnetic interactions operating in the spin-coupling process between the two copper centers increase with a decrease of the bridge angle (≤104°) and its distances.[1a,b] The very small $\mu_{1,1}$-azide-bridged Cu−N−Cu angles of 85.4(1)°, 87.2(1)° and Cu···Cu distances of 3.179(1) Å, 3.182(1) Å in **A** and **B** also indicate the existence of ferromagnetic coupling in complex **1**.

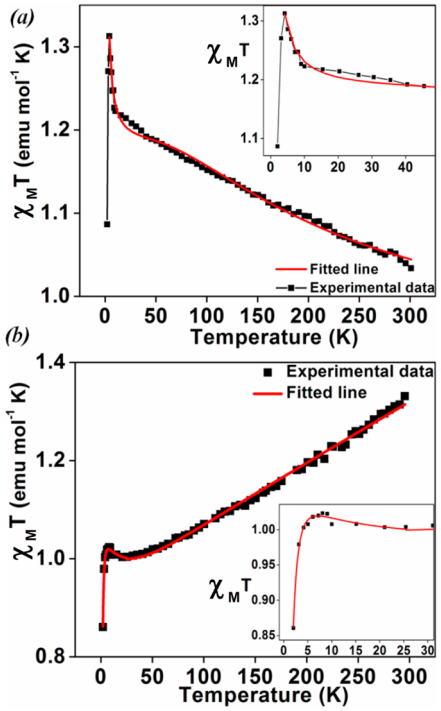

Figure 7. Variation of $\chi_M T$ value with temperature for (a) complex **1** and (b) complex **2**. Insets of both the Figures give the change in $\chi_M T$ value in the low-temperature region. The solid lines in red represent the theoretical curve obtained from eq 1

In complex **2**, the value of $\chi_M T$ decreases from 1.33 cm^3 mol^{-1} K to 1.01 cm^3 mol^{-1} K upon lowering the temperature until 40 K and remains almost constant down to 9 K and finally drops down to 0.86 cm^3 mol^{-1} K at 2 K (Figure 7b). The coupling constant, $2J$ obtained from the regression analysis is −24.7 cm^{-1}, signifying antiferromagnetic interaction between the two copper centers through azide bridges. This antiferromagnetic exchange coupling existing in the intradimer system is also well in agreement with the larger Cu···Cu distance of 3.426(1) Å and Cu−(μ_2-N_3)−Cu bridge angle of 102.5°, close to the limiting value for antiferromagnetic spin pairing.

The small bridge angle (Cu−(μ-NCS)−Cu) 85.5(1)° and the particularly short Cu···Cu distance (3.238(1) Å) in complex **3**, favors ferromagnetic exchange coupling between the copper(II) centers of the dimer. In this case, $\chi_M T$ increases from 0.72 to 0.80 cm^3 mol^{-1} K with decrease in temperature followed by a rapid drop to a value of 0.22 cm^3 mol^{-1} K below 45 K as shown in Figure S9 (SI). The coupling constant ($2J$) value extracted from the fitting procedure is +4.1 cm^{-1}, consistent with ferromagnetic exchange. The decrease of $\chi_M T$ value below 45 K suggests the presence of a weak antiferromagnetic intermolecular interaction which is taken into account with a Weiss correction term (θ = −0.4 K).

For complex **4**, $\chi_M T$ decreases continuously from 0.81 cm^3 mol^{-1} K to 0.79 cm^3 mol^{-1} K until temperature 20 K and falls rapidly in the lower temperature region to 0.57 cm^3 mol^{-1} K at 2 K (Figure S9, SI). The large intradimer Cu···Cu distance of 3.370(1) Å and the bridge angle of 100.4(8)° reveals an antiferromagnetic exchange between the copper(II) centers giving rise to a coupling constant value of $2J$ = −11.4 cm^{-1}.

Therefore, from the $\chi_M T$ versus T fitted curves it is seen that complexes **1** and **3** with very small bridge angles of 85.4−87.2° and shorter Cu···Cu distances (3.179(1), 3.182(1) Å, and 3.238(1) Å) possess ferromagnetic exchange interaction and complex **2** and **4** having larger bridge angles of >100° with larger Cu···Cu distances (3.426(1) and 3.370(1) Å) exhibit antiferromagnetic coupling.

To investigate the long-range ferromagnetic ordering, a field-dependent magnetization study (M−H) was carried out over the temperature range from 2 to 300 K. For complex **1** at lower temperature, in the low-magnetic field region, a very small coercivity of ∼20 Oe was obtained, but in the high-field region an abrupt increase in magnetic moment was observed both at positive and negative field region after 1 T with a prominent hysteresis loop as shown in Figure 8a. This field-induced magnetization was clearly shown in the inset of this figure. The field-induced ferromagnetism in complex **1** gives magnetic hysteresis curves at 2, 5, and 10 K. The effect is more prominent at 2 K and continues to be observed up to 10 K, above which the M−H behavior became almost linear and of paramagnetic type. From the $\chi_M T$ fit, it could be established that a weak ferromagnetic exchange coupling exists between the copper(II) centers.

Thus far in the literature, this type of strong field-induced ferromagnetism in dimeric metal complex systems having weak exchange coupling in the intradimers has not been reported. However, in some metal complexes, co-operative behavior of H-bonding or interaction between the metal centers via $\pi\cdots\pi$ stacking show this type of long-range ferromagnetic ordering at higher magnetic fields.[2b,24] Surprisingly, in complex (**1**), both

dx.doi.org/10.1021/ic501353g | Inorg. Chem. 2014, 53, 8723−8734

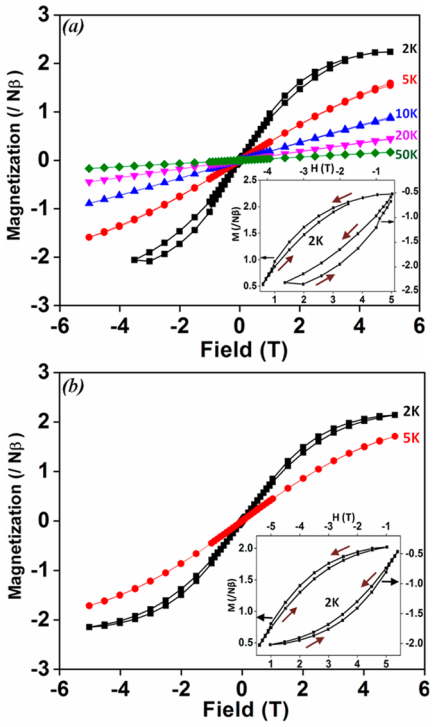

Figure 8. Magnetization vs magnetic field for (a) complex **1** and (b) complex **2**. Insets of both the a and b represent the field-induced ferromagnetic hysteresis loop at 2 K appearing after 0.9 T.

interactions are present. Therefore, to explain our results precisely, we attempted to separate these two different interactions by investigating three other "end-on" azide and thiocyanate-bridged dinuclear copper systems viz. **2**, **3**, and **4** where in particular **2** and **4** did not contain any N−H moieties for hydrogen-bond formation. In the structures it was found that complexes **2** and **3** possess $\pi\cdots\pi$ interactions between the interdimers. In addition to $\pi\cdots\pi$ interactions, complex **3** contains H-bonding interactions; however, complex **4** contains neither type of interaction. It is seen that at lower temperatures (up to 5 K) only complex **2** exhibits the strong field-induced ferromagnetic ordering at higher magnetic fields as shown in Figure 8b which is totally absent in complex **3** and **4** (Figure S10, SI). The inset of Figure 8b clearly shows the splitting in magnetization after 1 T. As H-bonding interactions are present in complexes **1** and **3** but only the former shows field-induced ferromagnetic ordering, it can be concluded that this field-induced ferromagnetism is distinctively operated via $\pi\cdots\pi$ stacking interactions. At the same time, although there are $\pi\cdots\pi$ interactions present in complexes **1**, **2**- and **3**, the field-induced phenomenon is found only in complexes **1** and **2**, while complex **3** shows pure paramagnetic like M−H behavior. This is because the distance between copper centers (S = 1/2) in two different dimers of complex **3**, between which the $\pi\cdots\pi$ interactions take place, is 12.133(2) Å which is far too large to produce effective field-induced ferromagnetic ordering. However, in complexes **1** and **2** the corresponding distances between the copper centers are much smaller at 5.947(1) and 8.690(4) Å, respectively. Figures 3, 4, and 6 clearly reveal the stacking interactions and the distances between the copper centers between which the $\pi\cdots\pi$ interactions take place of complex **1** [$D1_p$ = 3.249(2) Å, $D2_p$ = 3.512(2) Å], **2** [D_p = 3.834(1) Å, $D1_p$= 3.509(1)] and **3** [D_p = 4.001(2) Å, $D1_p$ = 3.362(1) Å], respectively. Although complex **2** exhibits the antiferromagnetic exchange coupling in the intradimers, the field-induced effect is dominated by π stacking interactions between the interdimers. The ferromagnetic ordering of magnetic moments for complexes **1** and **2** is also confirmed from the magnetization vs field plot as it shows the saturation magnetization value around 2.2 and 2.1/$N\beta$ respectively at 2 K. Due to the absence of long-range $\pi-\pi$ interaction (stacking) in complex **3**, responsible for the ferromagnetic ordering in the system, the magnetization moment in the M−H curve is not saturated at higher fields up to 5 T. In the case of complex **4**, no hysteresis loop is noticed even at high magnetic fields; however, an s-shaped curve is obtained as a result of long-range antiferromagnetic interactions.

Intermolecular magnetic coupling either ferromagnetic or antiferromagnetic owing to $\pi\cdots\pi$ interactions is well established.[3] To explain the field-induced ferromagnetism in complexes **1** and **2** we considered the presence of $\pi\cdots\pi$ stacking interactions between the π electron clouds of adjacent aromatic moieties. However, in the literature it is reported that at lower temperature, ferromagnetic ordering becomes stronger under high magnetic field which modifies the orientation of the molecules leading to interplanar π stacking interactions.[10] For our dinuclear systems, we have therefore considered that this long-range ferromagnetic ordering originated because of the enhancement of π stacking under the application of high magnetic fields preferably beyond 0.9 T. This "ordering magnetic field" is precisely shown in the derivative plot in Figure 9 giving rise to a transition peak at 0.9 T which is absent at higher temperatures. The shaded region giving the zone of hysteresis appears due to ferromagnetic ordering at higher magnetic fields. As the temperature increases, above 10 K for complex **1** and 5 K for complex **2**, the enhancement in the strength of the $\pi\cdots\pi$ stacking diminishes, and as a result, the field-induced ferromagnetism gradually disappears.

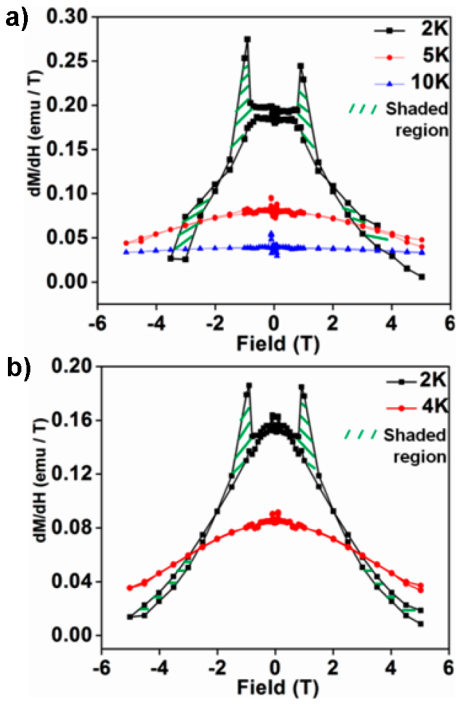

Figure 9. Peak appearing at 0.9 T in both the derivative plots indicates the ordering magnetic field for (a) complex **1** and (b) complex **2**. The shaded area (green line) arises as a result of hysteresis at higher fields.

dx.doi.org/10.1021/ic501353g | Inorg. Chem. 2014, 53, 8723−8734

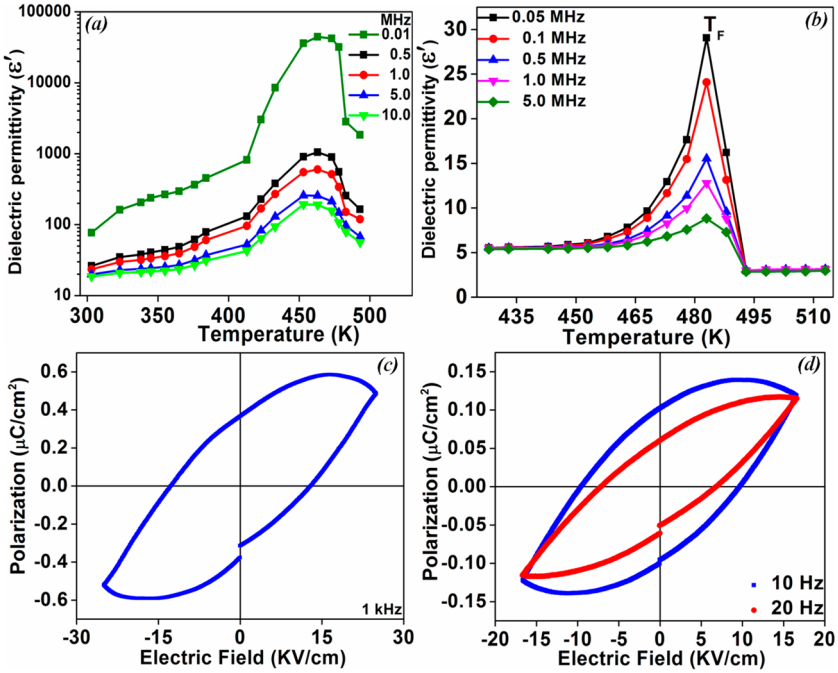

Figure 10. Representation of the ferroelectric transition temperatures obtained from the peak values of the dielectric curves as a function of temperature for (a) complex **1** and (b) complex **3**. The corresponding ferroelectric loops are shown in (c) and (d).

In the literature, similar examples of temperature-dependent spontaneous magnetization have been reported at low temperature and even at room temperature due to $\pi\cdots\pi$ interactions.[25,12] However, in this work, field-dependent or field-induced long-range ferromagnetic ordering in azide-bridged dinuclear complexes is observed for the first time.

3.5. Ferroelectric Response. Ferroelectricity is a collective phenomenon obtained in a system where there exists a long-range ordering of electric dipoles. To achieve this effect, the system needs to have permanent dipole moments to create spontaneous polarization which is reversed upon field reversal. Study of ferroelectricity in metal organic frameworks is currently a major area of research. The electric dipoles in metal organic frameworks mainly arise as a result of hydrogen bonds and chirality present in the system.[26] Among the present structures, only complex **1** exhibits both strong hydrogen bonds [H(26A)···O(11A) = 2.24 Å, H(26B)···N(1A) = 2.50 Å in molecule **A**, Figure 2, H(26E)···O(11B) 2.51, H(26F)···N(1B) 2.33 Å in molecule **B**] as well as chiral-centers [C(251) in molecules **A** (Figure 1) and **B** (Figure S1 in the SI) simultaneously].

To investigate the ferroelectric response due to spontaneous polarization of the dipoles, temperature-dependent dielectric measurements have been carried out for complex **1** over the temperature range from 298 to 490 K. Figure 10a shows the dielectric permittivity as a function of temperature at frequencies 0.5, 1, 5, and 10 MHz. It is seen that at all frequencies dielectric permittivity attains a peak at a temperature around 463 K, called ferroelectric transition temperature (T_F). Figure 10c gives the polarization hysteresis loop of complex **1** at room temperature (298 K). Remnant polarization (P_r) of 0.6 μC/cm^2 is obtained at 1 kHz. To examine the origin of this ferroelectricity, we have measured the polarization for complex **3** exhibiting a hydrogen-bonding effect between the dimers [H(26B)···O(11) = 2.36(3)Å, H(26A)···S(3) = 2.88(3) Å] as in complex **1**, but without any chiral atoms. Similar behavior of ferroelectric ordering is also found in complex **3**, as shown by the room temperature ferroelectric hysteresis loop given in Figure 10d. The remnant polarizations (P_r) of ∼0.11 and 0.05 μC/cm^2 are obtained at 10 and 20 Hz, respectively. Figure 10b shows the variation of dielectric permittivity with temperature for complex **3**, at frequencies of 0.05, 0.1, 0.5, 1, and 5 MHz. The ferroelectric transition temperature (T_F) for this complex is found at 483 K. The values of dielectric constants and its imaginary parts with frequency for complexes **1** and **3** are shown in Figure S12 in the SI. We have measured the leakage current for these two complexes **1** and **3** at room temperature to authenticate the ferroelectricity. The associated current values are found to be very low around 9.4 and 9.9 × 10^{-9} A/cm^2 respectively at an electric field of 1 kV/cm (Figure S11 in the SI). Basically, H-bonding supramolecular interactions present in these two complexes generate electric dipoles through intermolecular D−H$^{\delta+}\cdots$A$^{\delta-}$ moiety. In our case the H$^{\delta+}\cdots$N$^{\delta-}$ and H$^{\delta+}\cdots$S$^{\delta-}$ H-bonds present in complex **1** and complex **3** respectively possesses the electric dipole moment in their respective systems and form one-dimensional chains. Mainly these types of hydrogen-bonding structures show order−disorder-type phase transitions giving rise to peaks in dielectric permittivity as a function of temperature. Therefore, it is concluded that the source of this ferroelectric ordering present in systems **1** and **3** is the hydrogen bonds which form the one-dimensional chains as revealed from Figures 2 and 5, respectively. By contrast, however, the other complexes **2** and **4** do not display any ferroelectric response due to the absence of hydrogen bonds.

3.6. Magneto−Dielectric Behavior. The presence of field-induced ferromagnetism and ferroelectric ordering simultaneously in complex **1** develops multiferroicity in the system. In order to evaluate this behavior, magnetic field-dependent dielectric permittivity measurements have been carried out up to 2 T at room temperature. From Figure S13 in the SI, a moderate change in permittivity value is seen at the low

dx.doi.org/10.1021/ic501353g | Inorg. Chem. 2014, 53, 8723−8734

magnetic field region, while a significant change is observed (~8%) at higher fields beyond 0.8 T. Magnetic field-induced ferromagnetic ordering due to π stacking and the formation of electric dipoles through 1-D long-range H-bonding interaction are involved in the coupling process between the magnetic and electric dipoles which leads to multiferroic behavior in the system.

4. CONCLUSION

In conclusion, some new types of end-on pseudohalide-bridged dinuclear copper(II) complexes with N_2O donor tridentate Schiff base ligands are synthesized. Field-induced long-range ferromagnetic ordering is observed in compounds containing $\pi\cdots\pi$ stacking interactions, while compounds having hydrogen-bonding interactions give fairly good ferroelectric response. Most interestingly, complex **1** which contains both $\pi\cdots\pi$ stacking and hydrogen-bonding interactions shows unique multiferroic behavior which has potential applications in memory devices.

■ ASSOCIATED CONTENT

Ⓢ Supporting Information

Tables S1−S3, Figures S1−S14, and a CIF files giving a detailed description about the crystallographic data and magnetic interactions. This material is available free of charge via the Internet at http://pubs.acs.org."

■ AUTHOR INFORMATION

Corresponding Authors

*E-mail: shouvik.chem@gmail.com

*E-mail: cnssks@iacs.res.in

Author Contributions

⊥S.J. and B.K.S. contributed equally.

Notes

The authors declare no competing financial interest.

■ ACKNOWLEDGMENTS

This work was supported by the DST, India under FAST Track Scheme (Order No. SR/FT/CS-118/2010, dated 15/02/2012). S.J., B.K.S., and P.B. acknowledge CSIR, India (Fellowship for S.J., Sanction No. 09/096(0659)/2010-EMR-I, dated 18.1.11, Fellowship for B.K.S., Sanction No. 09/080(0764)/2011-EMR-1, dated 12.07.11 and Fellowship for P.B., Sanction No. 09/096(0607)/2010-EMR-I, dated 27.1.10). S.K.S. acknowledges DST, New Delhi, Govt. of India, Project No.: SR/NM/NS-1089/2011 for financial support. We thank the University of Reading and EPSRC (U.K) for funds for the diffractometer.

■ REFERENCES

(1) (a) Tandon, S. S.; Thompson, L. K.; Manuel, M. E.; Bridson, J. N. *Inorg. Chem.* **1994**, *33* (24), 5555−5570. (b) Thompson, L. K.; Tandon, S. S.; Manuel, M. E. *Inorg. Chem.* **1995**, *34* (9), 2356−2366. (c) Ruiz, R.; Julve, M.; Faus, J.; Lloret, F.; Munoz, M. C.; Journaux, Y.; Bois, C. *Inorg. Chem.* **1997**, *36* (16), 3434−3439. (d) Kahn, O. *Angew. Chem., Int. Ed.* **1985**, *24*, 834−850. (e) Ruiz, E.; Alemany, P.; Alvarez, S.; Cano, J. *J. Am. Chem. Soc.* **1997**, *119*, 1297−1303. (f) Laborda, S.; Clerac, R.; Anson, C. E.; Powell, A. K. *Inorg. Chem.* **2004**, *43*, 5931−5943.

(2) (a) Zeng, M.; Zhang, W.; Sun, X.; Chen, X. *Angew. Chem.* **2005**, *117*, 3139−3142. (b) Miyasaka, H.; Okawa, H.; Miyazaki, A.; Enoki, T. *Inorg. Chem.* **1998**, *37* (19), 4878−4883.

(3) Yoshizawa, K.; Hoffmann, R. *J. Am. Chem. Soc.* **1995**, *117*, 6921−6926.

(4) (a) Ribas, J.; Escuer, A.; Monfort, M.; Vicente, R.; Cortés, R.; Lezama, L.; Rojo, T. *Coord. Chem. Rev.* **1999**, *193−195*, 1027−1068. (b) Adhikary, C.; Koner, S. *Coord. Chem. Rev.* **2010**, *254*, 2933−2958. (c) Zeng, Y.-F.; Hu, X.; Liu, F.-C.; Bu, X.-H. *Chem. Soc. Rev.* **2009**, *38*, 469−480. (d) Triki, S.; Gómez-García, C. J.; Ruiz, E.; Sala-Pala, J. *Inorg. Chem.* **2005**, *44*, 5501−5508.

(5) (a) Fujita, W.; Kikuchi, K.; Mori, W. *Chem.—Asian J.* **2012**, *7*, 2830−2835. (b) Yin, P.; Zheng, L.-M.; Gaob, S.; Xina, X.-Q. *Chem. Commun.* **2001**, *22*, 2346−2347. (c) Pasán, J.; Sanchiz, J.; Ruiz-Pérez, C.; Campo, J.; Lloretd, F.; Julve, M. *Chem. Commun.* **2006**, *27*, 2857−2859. (d) Liu, T.-F.; Sun, H.-L.; Gao, S.; Zhang, S.-W.; Lau, T.-C. *Inorg. Chem.* **2003**, *42*, 4792−4794.

(6) (a) Burrows, A. D.; Mahon, M. F.; Sebestyen, V. M.; Lan, Y.; Powell, A. K. *Inorg. Chem.* **2012**, *51*, 10983−10989. (b) Uebler, J. W.; Stone, B. S.; LaDuca, R. L. *Z. Anorg. Allg. Chem.* **2013**, *639*, 1740−1745. (c) Marinho, M. V.; Simões, T. R. G.; Ribeiro, M. A.; Pereira, C. L. M.; Machado, F. C.; Pinheiro, C. B.; Stumpf, H. O.; Cano, J.; Lloret, F.; Julve, M. *Inorg. Chem.* **2013**, *52*, 8812−8819. (d) Zhu, M.; Su, S.-Q.; Song, X.-Z.; Hao, Z.-M.; Song, S.-Y.; Zhang, H.-J. *Dalton Trans.* **2012**, *41*, 13267−13270. (e) Willett, R. D.; Gómez-García, C. J.; Twamley, B. *Eur. J. Inorg. Chem.* **2012**, 3342−3348.

(7) Lazari, G.; Stamatatos, T. C.; Raptopoulou, C. P.; Psycharis, V.; Pissas, M.; Perlepes, S. P.; Boudalis, A. K. *Dalton Trans.* **2009**, *17*, 3215−3221.

(8) (a) Chandrasekhar, V.; Dey, A.; Das, S.; Rouzières, M.; Clèrac, R. *Inorg. Chem.* **2013**, *52*, 2588−2598. (b) Iasco, O.; Novitchi, G.; Jeanneau, E.; Luneau, D. *Inorg. Chem.* **2013**, *52*, 8723−8731. (c) Liu, J.-L.; Lin, W.-Q.; Chen, Y.-C.; Gómez-Coca, S.; Aravena, D.; Ruiz, E.; Leng, J.-D.; Tong, M.-L. *Chem.—Eur. J.* **2013**, *19*, 17567−17577.

(9) Dong, D.-P.; Liu, T.; Zheng, H.; Zhao, L.; Zhuang, P.-F.; He, C.; Duan, C.-Y. *Inorg. Chem. Commun.* **2012**, *24*, 153−156.

(10) Winter, S. M.; Cvrkalj, K.; Dube, P. A.; Robertson, C. M.; Probert, M. R.; Howard, J. A. K.; Oakley, R. T. *Chem. Commun.* **2009**, *47*, 7306−7308.

(11) (a) Ye, H.-Y.; Fu, D.-W.; Zhang, Y.; Zhang, W.; Xiong, R.-G.; Huang, S. D. *J. Am. Chem. Soc.* **2009**, *131*, 42−43. (b) Horiuchi, S.; Kumaia, R.; Tokura, Y. *Chem. Commun.* **2007**, *23*, 2321−2329.

(12) Giri, S.; Saha, S. K. *J. Phys. Chem. Lett.* **2011**, *2*, 1567−1571.

(13) Altomare, A.; Cascarano, G.; Giacovazzo, C.; Guagliardi, A.; Burla, M. C.; Polidori, G.; Camalli, M. *J. Appl. Crystallogr.* **1994**, *27*, 435−436.

(14) Sheldrick, G. M. *Acta Crystallogr.* **2008**, *A64*, 112−122.

(15) Spek, A. L. *J. Appl. Crystallogr.* **2003**, *36*, 7−13.

(16) *X-AREA and X-RED32* Stoe and Cie GmbH: Darmstadt, Germany, 2006; www.stoe.com.

(17) *Abspack*; Oxford Diffraction Ltd, Abingdon, UK, 2005.

(18) Gimeno, N.; Vilar, R. *Coord. Chem. Rev.* **2006**, *250*, 3161−3189.

(19) (a) Li, Z.-X.; Zhang, X.-L. *Acta Crystallogr.* **2004**, *E60*, m958−m959. (b) Karakas, A.; Elmali, A.; Unver, H.; Kara, H.; Yahsi, Y. *Z. Naturforsch.* **2006**, *61b*, 968−974.

(20) Jana, S.; Chattopadhyay, S. *Inorg. Chem. Commun.* **2013**, *35*, 160−163.

(21) Addison, A. W.; Nageswara, T.; Reedijk, J.; Rijn, J. V.; Verchoor, G. C. *J. Chem. Soc., Dalton Trans.* **1984**, 1349−1356.

(22) (a) Cremer, D.; Pople, J. A. *J. Am. Chem. Soc.* **1975**, *97*, 1354−1358. (b) Boeyens, J. C. A. *J.Cryst.Mol.Struct.* **1978**, *8*, 317−320.

(23) Bhowmik, P.; Jana, S.; Chattopadhyay, S. *Polyhedron* **2012**, *44*, 11−17.

(24) Chi, Y.; Yu, L.; Shi, J.; Zhang, Y.; Hu, T.; Zhang, G.; Shi, W.; Cheng, P. *Dalton Trans.* **2011**, *40*, 1453−1462.

(25) Li, L.-L.; Lin, K.-J.; Ho, C.-J.; Sun, C.-P.; Yang, H.-D. *Chem. Commun.* **2006**, *12*, 1286−1288.

(26) (a) Ye, H.; Fu, D.; Zhang, Y.; Zhang, W.; Xiong, R.; Huang, S. D. *J. Am. Chem. Soc.* **2009**, *131*, 42−43. (b) Dong, X.; Li, Bo.; Ma, B.; Li, S.; Dong, M.; Zhu, Y.; Zang, S.; Song, Y.; Hou, H.; Mak, T. C. W. *J. Am. Chem. Soc.* **2013**, *135*, 10214−10217. (c) Wang, Y.; Tang, G.;

Wan, W.; Wu, Y.; Tian, T.; Wang, J.; He, C.; Long, X.; Wang, J.; Ng, S. W. *CrystEngComm* **2012**, *14*, 3802−3812.